Earth and Planetary Science Letters 286 (2009) 89–100

Contents lists available at ScienceDirect

Earth and Planetary Science Letters

journal homepage: www.elsevier.com/locate/epsl

Spatial variations in effective elastic thickness in the Western Pacific Ocean and their implications for Mesozoic volcanism

L.M. Kalnins *, A.B. Watts

Department of Earth Sciences, University of Oxford, Parks Road, Oxford, OX1 3PR, UK

ARTICLE INFO

Article history:
Received 9 February 2009
Received in revised form 5 June 2009
Accepted 14 June 2009
Available online 22 August 2009

Editor: R.D. van der Hilst

Keywords:
elastic thickness
flexure
free-air gravity
bathymetry
submarine volcanism

ABSTRACT

We have used free-air gravity anomaly and bathymetric data, together with a moving window admittance technique, to determine the spatial variation in oceanic elastic thickness, T_e, in the Western Pacific ocean. Synthetic tests using representative seamounts show that T_e can be recovered to an accuracy of ± 5 km for plates up to 30 km thick, with increased accuracy of ± 3 km for $T_e \leq 20$ km. The Western Pacific has a T_e range of 0–50 km, with a mean of 9.4 km and a standard deviation of 6.8 km. The T_e structure of the region is dominated by relatively high T_e over the Hawaiian-Emperor Seamount Chain, intermediate values over the Marshall Islands, Gilbert Ridge, and Marcus-Wake Guyots, and low values over the Line Islands, Mid-Pacific Mountains, Caroline Islands, Shatsky Rise, Hess Rise, and Musician Seamounts. Plots of T_e at sites with radiometric ages suggest that T_e is to first order controlled by the age of the lithosphere at the time of loading. In areas that backtrack into the South Pacific Isotopic and Thermal Anomaly (SOPITA), T_e may be as low as the depth to the 180 ± 120 °C isotherm at least locally. In the northern part of the study area including the Hawaiian-Emperor Seamount Chain, T_e correlates with the depth to 310 ± 120 °C. These best-fitting isotherms imply peak rates of volcanism during 100–120 Ma (Early Cretaceous) and 140–150 Ma (Late Jurassic). The corresponding addition of 8×10^6 km^3 and 4×10^6 km^3 of volcanic material to the surface of the oceanic crust would result in long-term sea-level rises of 20 m and 10 m respectively. The Late Jurassic volcanic event, like the later Early Cretaceous event, appears to have influenced the tectonic evolution of the Pacific plate convergent boundaries, resulting in increased volcanism and orogenesis.

1. Introduction

The Western Pacific (Fig. 1) is home to a significant fraction of the world's Mesozoic seafloor, offering a window into the tectonic and volcanic environment of the Jurassic and Cretaceous oceans. Although this seafloor is characterised by many seamounts, ridges, and plateaux, relatively little is known about their tectonic setting. Age estimates are available from dredging, deep sea drilling, and sampling on ocean islands, but no information is available for many of the bathymetric features on the oldest seafloor. One parameter that is sensitive to the tectonic setting of a constructional submarine volcanic feature and does not require a physical rock sample is the effective elastic thickness of the lithosphere, T_e, a proxy for its long-term (i.e. 10^6 yr) strength.

Several different methods have been used to estimate T_e in the world's oceans, including measurements of flexure directly from seismic refraction data (e.g. Watts et al., 1985), geomorphic studies of the vertical motion history caused by flexure(e.g. McNutt and Menard, 1978), and, most commonly, spectral methods of analysing the relationship between the bathymetry and gravity or geoid anomaly (e.g. McKenzie and Bowin, 1976; Walcott, 1976). Previous studies have tended to focus on a particular geological feature, and the variety of methods used make it difficult to directly compare estimates and construct a regional or global map of T_e. Watts et al. (2006) used bathymetric prediction to determine T_e at over 9000 seamounts in the Pacific, Indian, and Atlantic oceans. However, their study is restricted to the relatively large, roughly circular seamounts and ocean islands in the Wessel (2001) database and does not attempt to estimate T_e over smaller or more irregularly shaped features, leaving T_e over much of the ocean unmapped.

Models of the conductive cooling of oceanic lithosphere suggest that its strength, as well as density and thickness, should increase with age. Watts (1978) suggested that oceanic T_e is to first order determined by the age of the lithosphere when a load such as a seamount is emplaced, and that this thickness is approximated by the depth to the 450 °C isotherm based on a cooling plate model (Parsons and Sclater, 1977). This relationship allows the approximate age of an unsampled bathymetric feature to be determined directly from the T_e and the age of the underlying seafloor. Later work has suggested that at least some regions follow a lower isotherm, 200-300 °C (e.g. Calmant and Cazenave, 1987; Goodwillie and Watts, 1993; Maia and

* Corresponding author. Tel.: +44 1865 282128; fax: +44 1865 272072.
E-mail address: lara.kalnins@earth.ox.ac.uk (L.M. Kalnins).

0012-821X/$ – see front matter © 2009 Elsevier B.V. All rights reserved.
doi:10.1016/j.epsl.2009.06.018

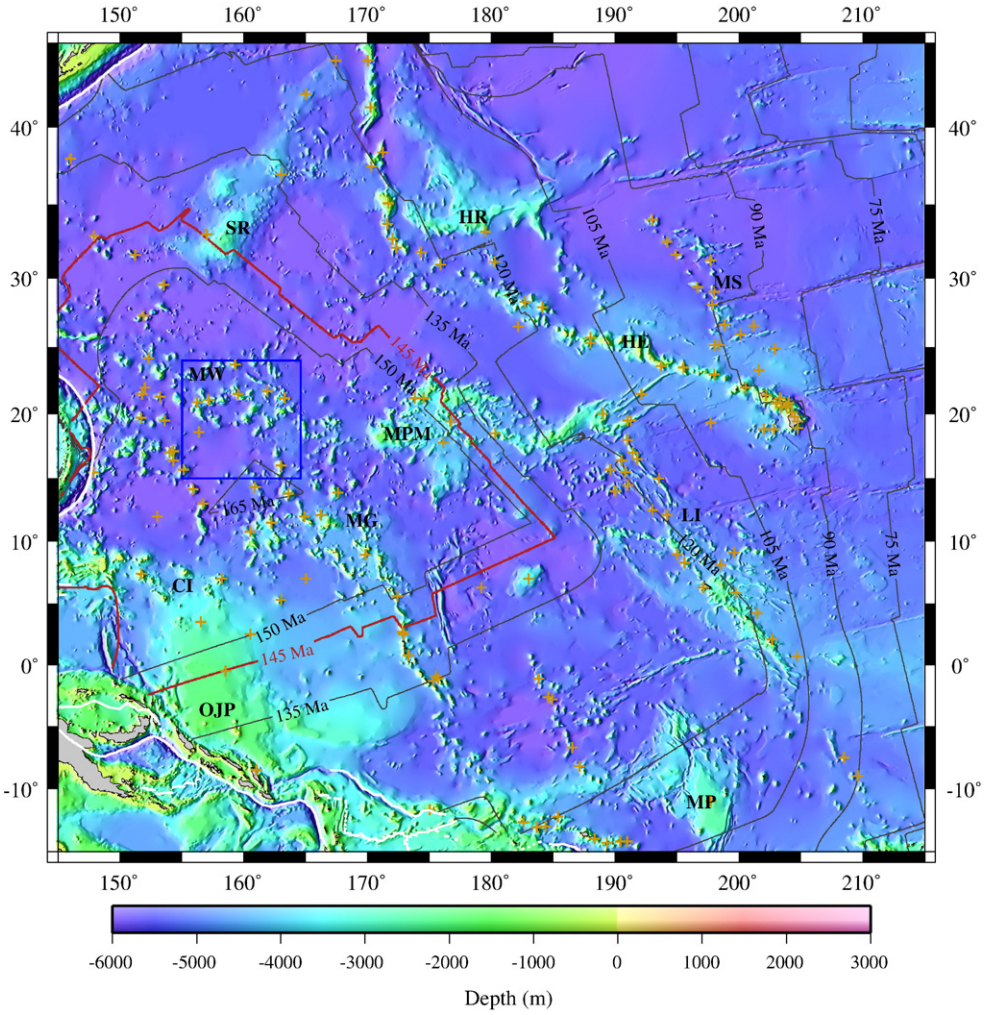

Fig. 1. Bathymetric map of the Jurassic and Cretaceous age Pacific Ocean based on the GEBCO 1×1 minute grid and seafloor age data from (Müller et al., 2008) showing selected features referred to in the text. The thick red contour marks the boundary between Jurassic and Cretaceous seafloor. Yellow crosses show the locations of dated samples (Clouard and Bonneville, 2005; Koppers and Staudigel, 2005) used to determine the lithosphere age at the time of loading. Plate boundaries are marked with a heavy white line. The blue box delineates the area used to calculate the admittance in Fig. 2. Bathymetric features: CI, Caroline Islands; HE, Hawaiian-Emperor Seamount Chain; HR, Hess Rise; LI, Line Island Chain; MG, Marshall Islands and Gilbert Ridge; MP, Manihiki Plateau; MPM, Mid-Pacific Mountains; MS, Musician Seamounts; OJP, Ontong-Java Plateau; SR, Shatsky Rise; MW, Marcus-Wake Guyots.

Arkani-Hamed, 2002), and that the relationship between T_e and age may be weak at best, at least at subduction zones where fracturing may significantly reduce the strength of the lithosphere (e.g. McNutt and Menard, 1982; Bry and White, 2007). These considerations suggest that it may not be possible to use a single controlling isotherm as a global guideline for oceanic T_e.

In this paper, rather than focus on a single geological feature, we determine T_e at sites across the Western Pacific using a moving window technique similar to those developed in order to map spatial variations in continental T_e (e.g. Lowry and Smith, 1994; Pérez-Gussinyé et al., 2004). We use the technique to re-evaluate the correlation between T_e and age at loading across the Western Pacific ocean, taking into account possible regional variations. A locally appropriate controlling isotherm is then used to assign an approximate age to bathymetric features and thus reconstruct the rate at which submarine volcanic material has been added to the plate through geological time. We have found that, in addition to the well-known 90–120 Ma volcanic event (e.g. Larson and Schlanger, 1981), which was associated with the formation of oceanic plateaux such as Ontong-Java, Shatsky, and Manihiki, there is a secondary peak of magmatic activity in the Western Pacific that corresponds approximately to the Jurassic-Cretaceous boundary (~145 Ma). This result is robust and does not depend on whether we assign a regional controlling isotherm or assume that all low T_e (<5–10 km) features formed on or near a spreading ridge.

2. Spatial variation using the moving window technique

We map the spatial variation in oceanic T_e using a moving window technique in which T_e is estimated for a small (400×400 km to 1400×1400 km) square window. The window is then shifted by 100 km, and the analysis is repeated to build up a regular grid of T_e estimates.

The characteristic wavelength of flexure varies with the strength of the lithosphere, and the amplitude varies with both T_e and the magnitude of the load (Watts, 2001). Because of this, the window size that should be used to recover T_e is not obvious. Too small a window can truncate the signal of features on stronger lithosphere, producing an artificially low T_e, e.g. truncating the "moat" around Hawaii (Fig. 1). Conversely, too large a window blends T_e across multiple features and tends to be biased towards the largest feature in the window, reducing the resolution of the grid. This is particularly noticeable along the Hawaiian-Emperor Seamount Chain, which has both a long wavelength and high amplitude of flexure. Perez-Gussinye and Watts (2005) address this problem in continental Europe by estimating T_e with a

range of window sizes and choosing the result from the window that best recovers the appropriate T_e value in synthetic tests. Here we instead combine the T_e estimates from six different window sizes ranging from 400×400 km to 1400×1400 km. Each estimate is weighted by the number of discrete wavenumbers with sufficient coherence to be used to fit T_e, a measure of both the data quality and the validity of the isostatic model in that window. The weighted estimates are then averaged to produce a final estimated T_e for the window.

In this paper we base our analysis on the 1×1 minute satellite-derived free-air gravity anomaly grid of Smith and Sandwell (1994, Version 16.1) and the GEBCO 1×1 minute shipboard bathymetry grid (IOC et al., 2003). The satellite-derived gravity offers better spatial coverage than shipboard gravity measurements. We prefer the GEBCO bathymetry because it does not contain any estimates derived from gravity data (e.g. Smith and Sandwell, 1994), thus guaranteeing the independence of the gravity and bathymetry data sets.

2.1. Admittance fitting for T_e

We compare in Fig. 2a an observed and theoretical admittance for a 1000×1000 km window centred on the Marcus-Wake Guyots (Fig. 1). The shape of the admittance function is dependent on the strength of the lithosphere, particularly in the diagnostic waveband of flexure where a "roll-over" from low to high admittance occurs. The observed admittance, $Z(\mathbf{k})$, can be defined in terms of the observed gravity anomaly, $G(\mathbf{k})$, and the observed bathymetry, $B(\mathbf{k})$, by (e.g. McNutt, 1979)

$$Z(k) = \frac{\langle G(\mathbf{k})\cdot B^*(\mathbf{k})\rangle}{\langle B(\mathbf{k})\cdot B^*(\mathbf{k})\rangle} \tag{1}$$

where k is the magnitude of the wavevector $\mathbf{k}$, $k=2\pi/\lambda$ where λ is the wavelength, * denotes the complex conjugate, and $\langle\ \rangle$ indicates annular averaging of the spectral estimates. The theoretical admittance is based on the flexure of an elastic plate overlying an inviscid substrate, given by (Watts, 2001)

$$Z(k) = 2\pi G(\rho_l-\rho_w)e^{-kd}\cdot\left\{1-\phi_e(k)\frac{(\rho_c-\rho_i)+(\rho_m-\rho_c)e^{-kt}}{(\rho_m-\rho_i)}\right\} \tag{2}$$

where G is the universal gravitational constant, d is the mean water depth, t is the mean crustal thickness, and ρ_w, ρ_l, ρ_i, ρ_c, and ρ_m are the densities of seawater, the topographic load, the material that infills the flexure, the lower crust, and the mantle respectively. ϕ_e is the elastic flexural response function defined by

$$\phi_e(k) = \left[\frac{Dk^4}{(\rho_m-\rho_i)g}+1\right]^{-1} \tag{3}$$

where g is the acceleration due to gravity and D is the flexural rigidity defined by

$$D = \frac{ET_e^3}{12(1-\nu^2)} \tag{4}$$

where E is Young's modulus and ν is Poisson's ratio.

Therefore, in addition to T_e, $Z(k)$ depends on the water depth, d, and the densities of the topographic load, ρ_l, and infill, ρ_i. These can be estimated by setting $\rho_i=\rho_l$ and applying Green's equivalent layer theorem to the admittance at wavelengths shorter than the isostatic roll-over, where the topography is largely uncompensated. The uncompensated admittance is given by (Watts, 2001)

$$Z(k) = 2\pi G(\rho_l-\rho_w)e^{-kd} \tag{5}$$

Other parameters assumed in the theoretical admittance calculations are given in Table 1.

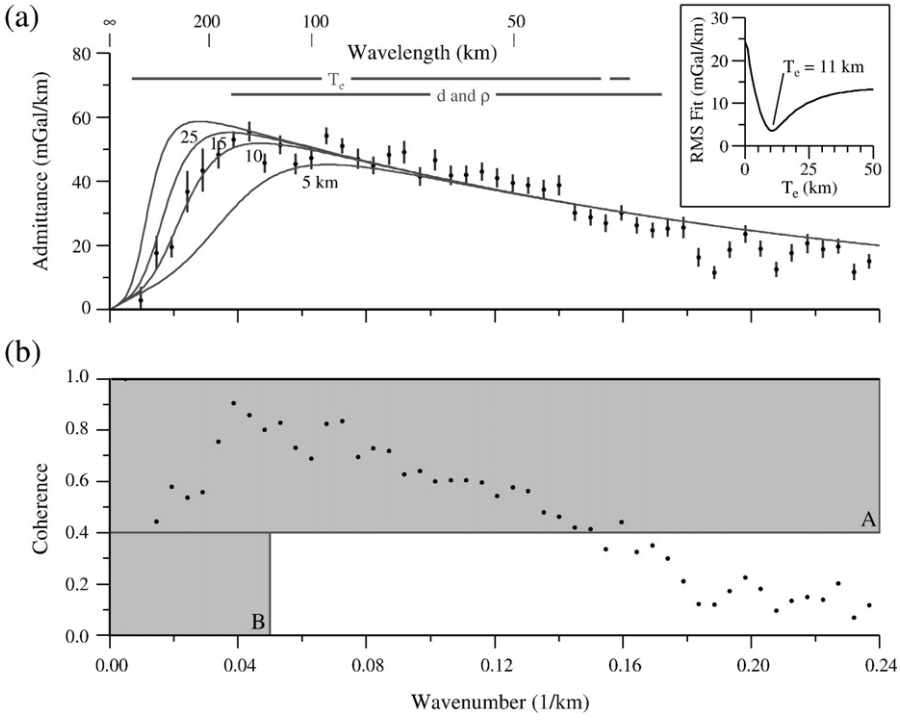

Fig. 2. Sample gravitational admittance and coherence used to determine T_e for the area within the blue box shown in Fig. 1. The coherence is used to determine which data points should be used in fitting the observed admittance. (a) Observed admittance with 1σ error bars and theoretical curves corresponding to T_e ranging from 5–25 km. Bars at the top of the figure indicate the data used in fitting T_e and in fitting the mean crustal density, ρ, and water depth, d, while the inset shows the RMS fit for T_e at this location. (b) Observed coherence with boxes showing the data used in fitting the admittance. Box A marks data where the coherence indicates that a significant portion of the free-air gravity anomaly is caused by the topography. Box B marks data below the coherence threshold of 0.4 that fall in the isostatic rollover where low coherence is predicted due to isostatic compensation.

Table 1
Summary of parameters assumed in admittance modelling.

Parameter	Notation in Equations	Value
Density of seawater	ρ_w	1030 kg/m^3
Density of lower crust	ρ_c	2900 kg/m^3
Density of mantle	ρ_m	3330 kg/m^3
Mean crustal thickness	t	8.0 km
Young's modulus	E	100 GPa
Poisson's ratio	ν	0.25

In order to compare the observed and theoretical admittances, we first use the coherence, γ^2, between the bathymetry and gravity anomaly to determine the range of wavenumbers to fit. The coherence is given by (e.g. McKenzie and Bowin, 1976)

$$\gamma^2(k) = \left\langle \frac{|S_{BG}(\mathbf{k})|^2}{S_{BB}(\mathbf{k})S_{GG}(\mathbf{k})} \right\rangle \tag{6}$$

where S_{BG} denotes the cross-power spectrum of the gravity and bathymetry, S_{BB} and S_{GG} denote the auto-power spectra of the bathymetry and gravity respectively, and $|\ |$ denotes magnitude.

High coherence indicates that a large portion of the gravity anomaly is caused by the bathymetry, an important assumption of our model. Wavenumbers with γ^2 over the threshold of 0.4 show sufficient coherence to be used in fitting T_e; in addition, low wavenumbers from the isostatic rollover, where the isostatic model predicts a low coherence, are also used (Fig. 2b).

Using the best-fitting d and ρ_l, theoretical admittance curves may then be calculated for a range of T_e and compared with the observed values at the selected wavelengths. The T_e at the RMS minimum is then assigned to the centre of the window(Fig. 2b inset). For the window used in Fig. 2, we derive a best-fitting d of 5260 m, ρ_l of 2710 kg/m^3 and T_e of 11 ± 2 km. Tests using a range of likely estimates of the thickness of oceanic crust (4–16 km) have an effect of + 2/-1 km on the estimated T_e. This is within error, so we conclude that the assumption of a constant t of 8 km is reasonable. The d is within 100 m of the actual median bathymetry in the window, while the ρ_l is within the range of previous estimates of the density of oceanic "layer 2" (e.g. Carlson and Raskin, 1984). The T_e is moderate and suggests a tectonic setting on either a slow spreading ridge crest or a ridge flank.

2.2. Synthetic data and finite window biasing

In order to validate T_e derived using the moving window technique, we created a synthetic bathymetry grid composed of randomly distributed Gaussian-shaped seamounts, constructed to match the characteristics of natural seamounts (Fig. 3a). The bathymetric loads were then assigned a constant T_e and allowed to flex the lithosphere, assuming the same constants as used in the theoretical admittance calculation (Table 1). The load and resulting flexure were then used to calculate the associated free-air gravity anomaly (Fig. 3b). Randomly distributed noise was added to mimic instrument error and any incoherence between gravity and bathymetry due to subsurface loading. We then used the synthetic bathymetry and calculated gravity anomaly, together with the moving window technique, to recover T_e across the grid (Fig. 3c).

Fig. 3d shows the mean T_e recovered across the grid using the weighted average of all six window sizes for an input T_e ranging from 0 to 50 km. The insets show the mean T_e recovered by each window size as well as by the weighted average of all six window sizes and by the weighted average of the three largest window sizes for the representative input values $T_e = 5$ km and $T_e = 35$ km.

For low T_e ($\leq$10 km), Fig. 3 shows that all window sizes recover a consistent T_e, but as T_e increases, the standard deviation increases markedly for windows $\leq 800 \times 800$ km. The increase is particularly dramatic for the 400×400 km window; although it recovers a slightly higher mean T_e than many of the other window sizes, two standard deviations span the entire range of T_e tested from 0 to 50 km. The smallest window is thus unsatisfactory for recovering moderate to high values of T_e, and the 600×600 km and 800×800 km windows are of limited use. However, the smaller windows can better resolve sharp changes in T_e (Pérez-Gussinyé et al., 2004) and sometimes recover T_e in areas where the larger windows cannot, particularly those with small features, low T_e, and coherence near the lower limit of 0.4. This prevents us from discarding the smaller windows entirely, but requires that their effect be minimised in high T_e windows. The weighted average naturally achieves this because the larger window size allows the calculation of more closely spaced wavenumbers, increasing the number of admittance values used for fitting T_e in those windows and thus weighting the larger windows more heavily in the average. This minimises the effect of erratic results from the smaller window sizes, as can be seen by comparing the weighted averages for all six windows with those for the three large windows (Fig. 3d).

We found that while the mean T_e recovered by the weighted average of all six windows is consistent, it is about 20% lower than the input T_e. This bias is introduced, we believe, by the windowing of the observed bathymetry and gravity. Windowing the observed data has the effect of convolving both the bathymetry and free-air gravity anomaly with the windowing function before the admittance is calculated. The observed admittance then becomes

$$Z(k) = \frac{\langle (G(\mathbf{k}) * W(\mathbf{k})) \cdot (B(\mathbf{k}) * W(\mathbf{k}))^* \rangle}{\langle (B(\mathbf{k}) * W(\mathbf{k})) \cdot (B(\mathbf{k}) * W(\mathbf{k}))^* \rangle} \tag{7}$$

where W is the spectral representation of the windowing function and $*$ denotes convolution.

By contrast, the theoretical admittance defined in Eq. (2) assumes an infinite window, which corresponds to the admittance as defined in Eq. (1). The windowing function artificially shortens the longer wavelengths, displacing the observed admittance relative to the theoretical and thus downward biasing the recovered T_e. This phenomenon has been previously described by Pérez-Gussinyé et al. (2004) in continental studies and produced a similar downward bias of T_e estimates.

Fig. 3d shows that the bias is predictable and therefore a correction can be calculated and applied. Once the correction is applied to the raw T_e recovered from the synthetic data, the small standard deviation allows us to recover the input T_e with good precision. The only exception to the downward bias is for $T_e < 1$ km, which recovers an anomalously high T_e. However, even a fast spreading ridge is expected to have a $T_e \geq 2$ km at the ridge crest (Cochran, 1979), so such an extremely low T_e should occur only rarely, perhaps where a fast spreading ridge and hotspot coincide. These considerations suggest that so long as we use the same suite of finite window sizes, the correction can be applied to the T_e recovered from observations throughout the Western Pacific.

3. Results

Fig. 4 shows the T_e recovered across the Western Pacific before and after the correction from Section 2.2 is applied. The patterns in the spatial variations of T_e show a high correlation with individual geological features. Among the most striking is the swath of moderate to high corrected T_e (10–30 km) along the Hawaiian-Emperor Seamount Chain. The highest values of T_e occur around the Hawaiian Islands; T_e then monotonically decreases, past the bend in the chain, to the southern Emperor Seamounts. This is consistent with an intraplate origin for the Hawaiian-Emperor Seamount Chain and their formation on old, strong oceanic lithosphere. T_e along the northern Emperor Seamounts varies less systematically, but appears to be influenced by

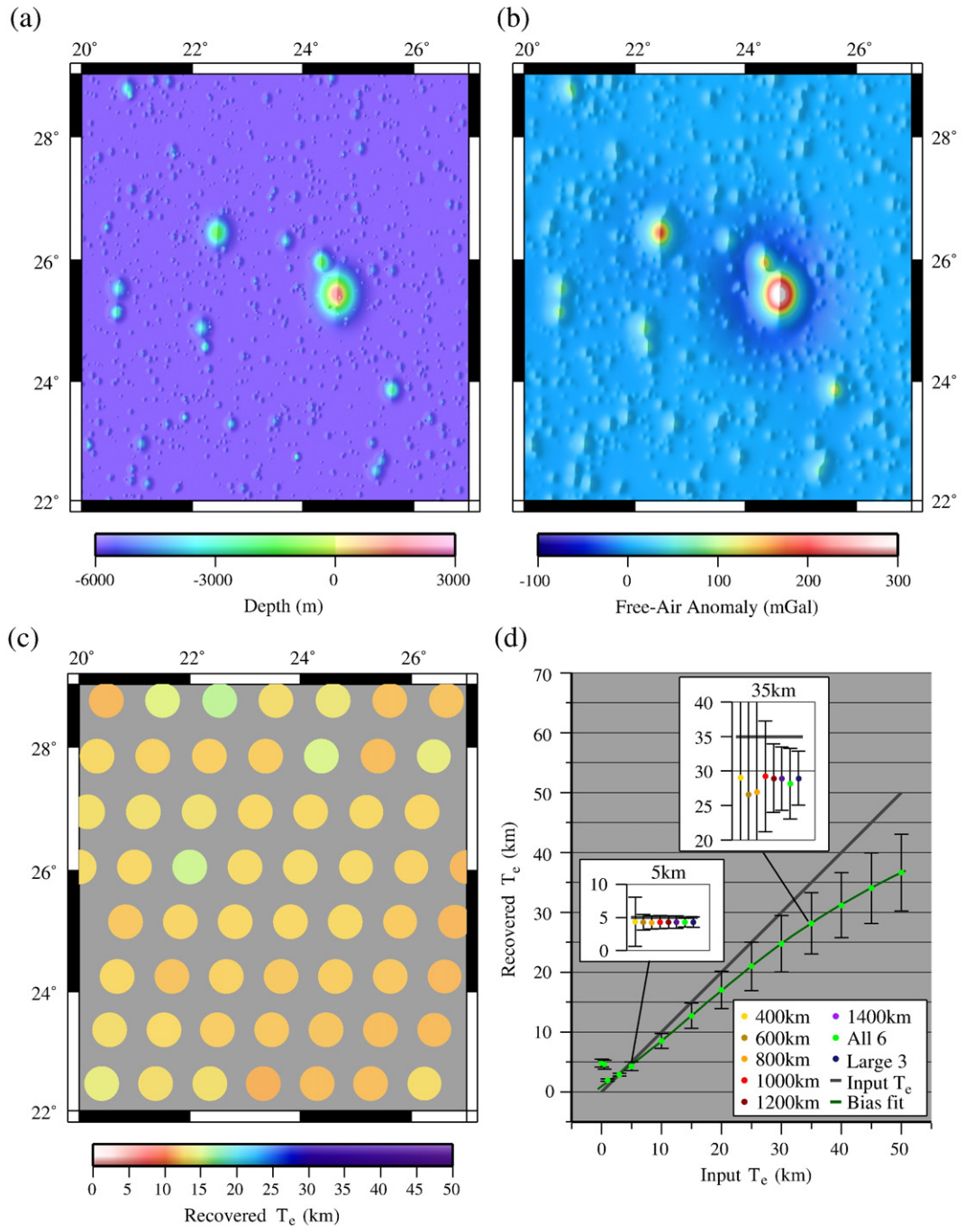

Fig. 3. Synthetic bathymetry and gravity data used to test the moving window technique and calibrate a correction curve to compensate for the downward bias caused by the finite window sizes. (a) Section of synthetic bathymetry composed of Gaussian seamounts. (b) Synthetic free-air gravity anomaly for $T_e = 15$ km. (c) Best-fitting T_e from the moving window technique. The size of each circle scales with the number of high coherence wavebands in that window, which is essentially uniform here. (d) Mean recovered T_e with 2σ error bars versus input T_e using a weighted average of all six window sizes ranging from 400–1400 km. The green line shows the best-fitting bias correction curve. Insets for $T_e = 5$ km and $T_e = 35$ km show averages and error bars for individual window sizes together with the weighted averages for all six windows and the largest three windows.

the high values recovered over the cluster of unnamed seamounts to the east of the northern part of the Shatsky Rise.

The Hawaiian-Emperor Seamount Chain also demonstrates how using windows hundreds of kilometres in width smears out the spatial variations in T_e. The swath of high T_e following the Hawaiian-Emperor Seamount Chain extends approximately 500 km on either side of the seamounts themselves (Fig. 4). This can produce incorrect results over smaller, older features within the swath such as the southern Musician Seamounts. This is because the flexure around the smaller features is of lower amplitude and shorter wavelength than that around the Hawaiian-Emperor Seamounts, so the admittance is dominated by the signal from Hawaii, rather than by the signal from the local features. In the case of the southernmost Musician Seamounts, this means that they appear to have a T_e of up to 25 km, in sharp contrast to the more northern Musician Seamounts, which have a very low T_e (3–7 km). This is compatible with the results of Freedman and Parsons (1986), who found a best-fitting T_e of 5 km for all the Musician Seamounts. The square pattern of the highest T_e values

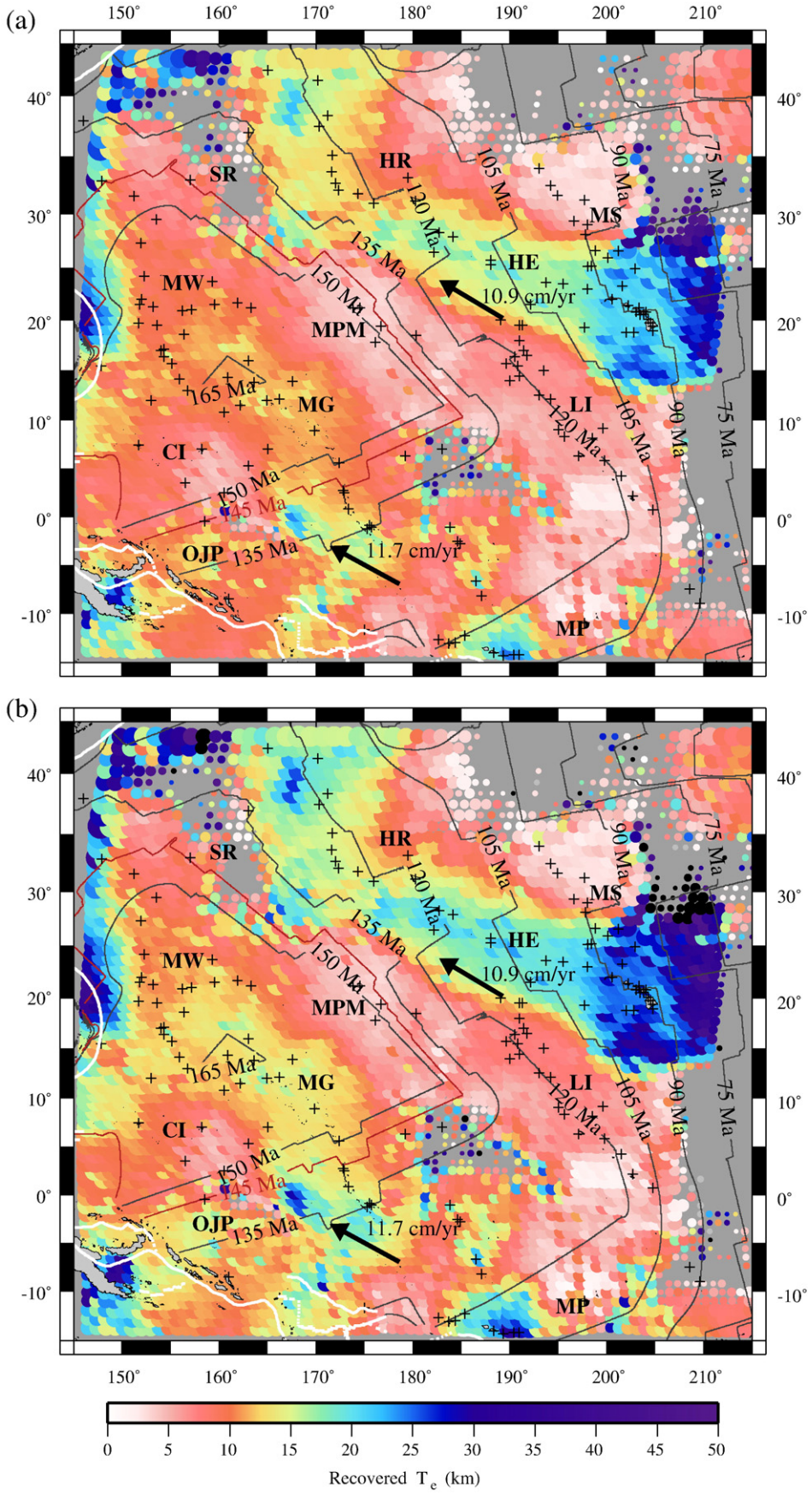

Fig. 4. Recovered T_e over the Western Pacific. Age contours, sample locations, plate boundaries, and feature labels are as described in Fig. 1. Heavy black arrows indicate plate motion in a hotspot reference frame (Gripp and Gordon, 2002). Circle size for each data point scales as described in Fig. 3. Blank areas in the map indicate regions with insufficient coherence to determine T_e at any window size. (a) Raw recovered T_e. (b) Recovered T_e after the bias correction from Fig. 3d is applied.

around the Hawaiian Islands, especially to the south and east, is also an artefact of the geographical extent and shape of the windows.

We also see a distinct pattern of spatial variation along the Marshall Islands, Gilbert Ridge, and Marcus-Wake Guyots. This pattern is especially clear in the corrected T_e (Fig. 4b), which shows a band of moderate T_e (12–17 km) along these seamounts. Although less pronounced than the trend along the Hawaiian-Emperor Seamount Chain, T_e monotonically decreases from the southern end of the Marshall Islands to the Marcus-Wake Guyots in the north. This is again broadly consistent with results from Ar/Ar dating (Ozima et al., 1977; Ozima et al., 1984; Davis et al., 1989; Smith et al., 1989; Lincoln et al., 1993; Pringle et al., 1993; Winterer et al., 1993; Koppers et al., 2000) and seafloor age (Müller et al., 2008), which show that the Marshall Islands, Gilbert Ridge, and Marcus-Wake Guyots formed on lithosphere 30–90 Myr old.

Other seamounts, including the Line Islands, the Caroline Islands, the Musician Seamounts, and the Mid-Pacific Mountains, all show a low T_e (<10 km). Although some of these features, such as the Musician Seamounts, did form on relatively young lithosphere (Sager and Pringle, 1987; Pringle, 1993), as suggested by their low T_e, others, such as the Caroline Islands and the Line Islands, formed on lithosphere that was significantly older (Lanphere and Dalrymple, 1976; Saito and Ozima, 1976; Saito and Ozima, 1977; Keating et al., 1984a; Keating et al., 1984b; Schlanger et al., 1984; Davis et al., 2002). This suggests either that this lithosphere has not increased in strength with age or that the low T_e reflects an early large-volume volcanic event while the sample age indicates a later small-volume event (e.g. Natland and Winterer, 2005).

In addition to T_e over seamounts, we also recover a pattern of high T_e over the outer rise seaward of the Japan, Izu-Bonin, and Mariana trenches and at the northernmost tip of the Tonga-Kermadec trench. These high values suggest that the subducting Pacific plate remains relatively strong as it bends down into the trench, and that weakening due to fracturing may not be as significant as previously supposed (e.g. McNutt and Menard, 1982; Bry and White, 2007). However, our theoretical admittance is computed assuming only surface loads and does not take into account subsurface loads, such as those due to a dense down-going slab. Further synthetic tests (e.g. Section 2.2) incorporating the bathymetry and free-air gravity anomaly characteristic of a subduction zone are required to determine the reliability of these results.

We also recover a pattern of low T_e over oceanic plateaux, including the Ontong-Java Plateau, the Manihiki Plateau, the Hess Rise, and the Shatsky Rise. The uniformly low T_e seen over the oceanic plateaux may reflect their formation at a spreading centre (e.g. Mahoney et al., 2005, Shatsky Rise). Alternatively, a thermal anomaly associated with the formation of the plateau (e.g. Gladczenko et al., 1997, Ontong-Java Plateau) or with the rifting of conjugate plateaux (e.g. Taylor, 2006, Manihiki, Hikurangi, and Ontong-Java Plateaux) may significantly weaken the overlying lithosphere, effectively resetting it to near zero age. This may also explain the low T_e recovered over the nearby Caroline Islands. Although the southern half of the Ontong-Java Plateau shows an intermediate T_e of 10–15 km, this may be influenced by the old subduction zone along the Vityaz Trench to the south.

Finally, we have recovered some 4400 estimates of the density of the uppermost oceanic crust in the Western Pacific. The density estimates and their relationship with oceanic crustal age are summarised in Appendix A.

4. Discussion

4.1. Relationship between T_e and the age of the lithosphere at the time of loading

Previous oceanic flexure studies (e.g. Watts, 1978; Calmant et al., 1990; Maia and Arkani-Hamed, 2002) suggest that the strength of the lithosphere at seamounts and ocean islands depends strongly on the age at the time when the volcanic load is emplaced. However, the precise relationship recovered between T_e and age at loading varies, with T_e variously described by depths ranging from the 200 °C isotherm (Maia and Arkani-Hamed, 2002, Foundation Seamounts), through the 450 °C isotherm (Watts, 1978, Hawaiian Chain), to the 600 °C isotherm (McNutt and Menard, 1982, oceanic trenches; Wessel and Haxby, 1990, Pacic fracture zones). This suggests that there is no single isotherm that controls T_e on a global scale, although a single isotherm may be a useful regional model.

In recent years, there has been a significant improvement in the number of reliable radiometric sample ages at seamounts and ocean islands (e.g. Clouard and Bonneville, 2005; Koppers and Staudigel, 2005), which allows us to better constrain the regional controlling isotherms. Within the study area, there are approximately 150 sample sites, which can be assigned a T_e from our corrected grid. Fig. 5 shows the corrected T_e versus the age of the lithosphere at the time of loading (i.e. the difference between the seafloor age (Müller et al., 2008) and the sample age).

Before evaluating the regional controlling isotherm, we have removed approximately 20 sample sites that we believe have been affected by the smearing out of spatial variations in T_e. These are sites that lie in the broad swath of high T_e that surround both the Hawaiian-Emperor Seamount Chain (Fig. 4) and the outer rises of subduction zones. These sites will therefore pair the age at loading calculated from the local sample and seafloor ages with a T_e dominated by regional features that do not share the local ages.

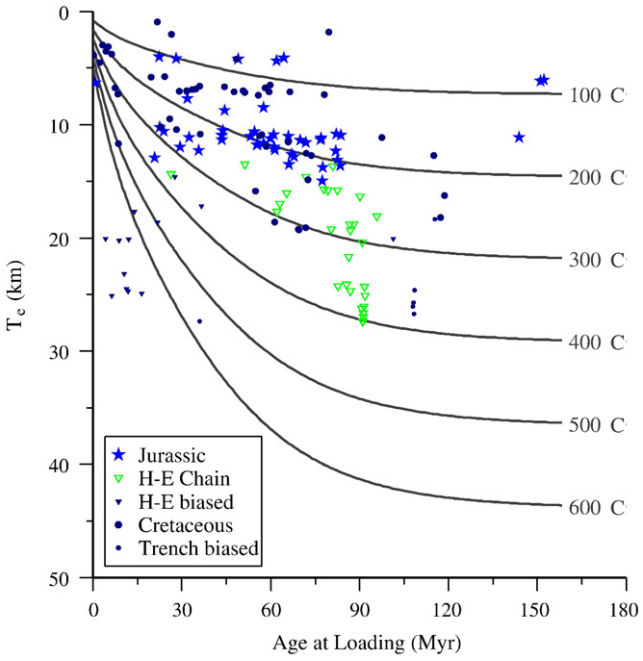

Fig. 5. Corrected T_e versus lithosphere age at the time of loading. Blue stars indicate features on Jurassic age seafloor, with an envelope of approximately 50-300 °C. Large green inverted triangles indicate features in the Hawaiian-Emperor Seamount Chain with an envelope of 200-400 °C; dark blue inverted triangles indicate features not part of the chain but falling within the broad swath of T_e heavily influenced by the Hawaiian-Emperor Seamount Chain (Fig. 4), and thus pair the T_e of the Hawaiian-Emperor Seamount Chain with their own age at loading. Large dark blue circles indicate results from other features, generally on Cretaceous seafloor, corresponding to an envelope of 0–300 °C. Small dark blue circles indicate features whose apparent T_e is likely influenced by the T_e of the down-going slab of a nearby trench. Isotherms are based on a cooling plate model with a plate thickness of 95 km, thermal diffusivity of 32 km^2/Myr, and temperatures of 0 °C and 1300 °C at the upper and lower plate boundaries respectively.

The most striking example is the southern Musician Seamounts discussed in Section 3, whose low age at the time of loading (<20 Myr) and high apparent T_e (20–25 km) from the Hawaiian Emperor Seamount Chain places them considerably deeper than the 600 °C isotherm (Fig. 5). A similar effect has been observed at Samoa (age at the time of loading of ~110 Myr) near the northern tip of the Tonga-Kermadec Trench (T_e of ~25 km), which plots between the 300 °C and 400 °C isotherms. We therefore believe that the smeared points are artefacts of our spectral windowing technique, and so we have excluded them from the analysis of regional controlling isotherms.

Other sources of scatter exist in plots of T_e versus age at the time of loading. Probably the most important is that a sample age may not represent the full volcanic history of an individual bathymetric feature. For example, the Line Islands experienced near-synchronous volcanism along the length of the chain first at 90 Ma, then again at 70 Ma, followed by further volcanism in the centre of the chain at 37 Ma (Davis et al., 2002). The recovered T_e will reflect the time when the bulk of the feature was emplaced, most likely the 90 Ma event, while the actual sample ages may be considerably younger. Even with a feature formed in single period of volcanism, the sample age will most likely correspond to the end of the volcanism, while the T_e will probably correspond to a slightly earlier time when the bulk of the submarine volcanic edifice was emplaced. This effect will downward bias the apparent controlling isotherm by matching the recovered T_e with too high an age at the time of loading. In the case of the Line Islands, if the T_e of 5–10 km corresponds to the 90 Ma event, the islands have an age at loading of 30 Myr and plot between the 150 °C and 250 °C isotherm. If the T_e corresponds to the 37 Ma event, the age at loading is 83 Myr and the islands plot between the 50 °C and 150 °C isotherm. This demonstrates that multiple episodes of volcanism can have a significant effect on the apparent controlling isotherm.

Additional sources of scatter include weakening due to thermal reheating and rejuvenation of the lithosphere (Calmant and Cazenave, 1986) and an increase in curvature due to fracturing and faulting of deformed lithosphere (McNutt, 1984), both of which act to reduce T_e, such that the lithosphere appears weaker than it should be on the basis of its age alone.

Another source of weakening is load-induced viscoelastic stress relaxation (Watts and Zhong, 2000). This may explain our results along the Hawaiian Ridge, which has a relatively constant age at the time of loading, and yet T_e monotonically increases from the oldest loads (e.g. Midway) to the youngest ones (e.g. Hawaii). For young loads that have not yet relaxed, the lithosphere can thus appear stronger than it should be on the basis of age.

These considerations of the sources of scatter in plots of T_e versus age at loading suggest that we can subdivide the Western Pacific seafloor into three regions (Fig. 5): Jurassic (★), the Cretaceous excluding the Hawaiian-Emperor Seamount Chain (●), and the Hawaiian-Emperor Seamount Chain (▽). The figure shows that bathymetric features formed on Jurassic age seafloor have an envelope of 50-300 °C, with a best fit of 180 °C with a standard deviation of 3 km. This corresponds to a 95% confidence interval with a controlling isotherm of 180 °C ± 90 °C. The Cretaceous, however, is characterised by two distinct populations: the Hawaiian-Emperor Seamount Chain, which has an envelope of 200-400 °C with a best fit of 310° ± 120 °C, and the remaining seamounts and ocean islands, which have an envelope of 0-300 °C with a best fit of 180 °C ± 120 °C. We conclude from these results that the T_e structure of Jurassic and Cretaceous oceanic lithosphere is similar, such that bathymetric features are associated with a T_e given approximately by the depth to the 180 °C isotherm based on a cooling plate model. The notable exception is the Hawaiian-Emperor Seamount Chain, which is associated with a significantly higher controlling isotherm.

We have found that T_e is in the range of 13–27 km along the Hawaiian Ridge, which extends from Loihi in the east to Abbott Seamount near the bend in the chain. This is similar to previous estimates based on shiptrack gravity data (18–37 km — Watts, 1978) and satellite altimeter-derived geoid data (21–33 km — Calmant, 1987). Watts and ten Brink (1989) and Wessel (1993) obtained a higher value of 40 km using seismic reflection profile data. However, Watts and ten Brink (1989) attributed the high value to unbending of the lithosphere due to magmatic underplating. The negatively buoyant underplating is generally coherent with the surface volcanic load but has a longer wavelength. This gives the appearance of a surface load on stronger plate, resulting in a higher apparent Te. Watts and ten Brink (1989) estimated a corrected T_e of approximately 25 km accounting for both the surface and subsurface loading.

The question that remains, then, is why other volcanic features near the Hawaiian-Emperor Seamount Chain that are on Jurassic and Cretaceous oceanic lithosphere follow a significantly lower controlling isotherm. Possible sources of the difference include successive volcanic events at a single feature or fundamental differences in the thermal and mechanical evolution or formation of the underlying lithosphere. Previous studies have found a controlling isotherm of less than 300 °C over the Cook, Austral,and Pitcairn-Mururoa-Gloucester seamount chains (Calmant, 1987), and have attributed this isotherm to the formation of these features in the region of the South Pacific Isotopic and Thermal Anomaly (SOPITA) (e.g. Staudigel et al., 1991). This region is characterised by unusually shallow seafloor and has been dubbed by McNutt and Fischer (1987) the Pacific "superswell". We note that many of the features in the southern and western parts of our study area, including the Mid-Pacific Mountains, the Marcus-Wake Guyots, the Marshall Islands, the Gilbert Ridge, and the Line Island Chain, backtrack along Pacific absolute motion paths into SOPITA (e.g. Smith et al., 1989).

Goodwillie and Watts (1993) and Jordahl et al. (2004) pointed out that T_e at a number of seamounts and oceanic islands in SOPITA (e.g. Gambier, Marquesas, and the Cook-Austral Islands) that were thought by Calmant (1987) to plot with a low controlling isotherm now plot within "normal" isotherms (300–600 °C). Nevertheless there are still a number of features in the "superswell" region (e.g. Pitcairn, Rarotonga (Goodwillie and Watts, 1993), and the Foundation Seamounts (Maia and Arkani-Hamed, 2002)) that plot with a low controlling isotherm. In addition, lower values such as those obtained by Calmant (1987) cannot be definitively ruled out for the Cook-Austral Islands (Jordahl et al., 2004). These considerations suggest that lithosphere formed over SOPITA may therefore be thinner and weaker at least locally. The controlling isotherm data (Fig. 5) suggest that a region of weakened lithosphere extends northwest of SOPITA as far as the Marcus-Wake Guyots and the Mid-Pacific Mountains, implying that isotopic and thermal anomaly is a long-lived feature, persisting over 100 Myr.

The fact that the Hawaiian-Emperor Seamount Chain is associated with a higher controlling isotherm of approximately 300 °C is thus consistent with its formation away from SOPITA. Features near the Hawaiian-Emperor Seamount Chain, such as the Musician Seamounts and the Hess Rise, also formed away from SOPITA, but they share a low age at the time of loading, making it difficult to determine their controlling isotherms. In previous studies, Parmentier and Haxby (1986) and Wessel and Haxby (1990) found a controlling isotherm of 600-700 °C based on geoid anomalies at Pacific fracture zones. In addition, McNutt and Menard (1982) used shiptrack gravity and bathymetry data over the outer rise seaward of trenches and found a controlling isotherm of 550-600 °C after correcting for curvature and yielding. This suggests that while the controlling isotherm along the Hawaiian-Emperor Seamount Chain appears high relative to the rest of the study area, it may be low compared to the isotherms for lithosphere that has not been modified by a long-lived mantle plume.

4.2. Rate of volcanism and sea-level change in the Mesozoic

Determination of the regional controlling isotherm allows us to use T_e to estimate the age of an individual bathymetric feature, providing that the age of the underlying seafloor is known. In our study area, there are over 1800 seamounts, banks, and rises that stand more than 1500 m above regional seafloor depths (Hillier and Watts, 2007), of which only 150 have been sampled. Our grid, based on T_e estimates in over 4400 unique windows, therefore allows us to assign approximate ages to the many undated features in the Western Pacific. The Jurassic seafloor, for example, has a particularly high concentration of seamounts and oceanic islands, most of which have a low to intermediate T_e, suggesting an unusually high level of submarine volcanism in the Jurassic and Cretaceous when this lithosphere was young.

The choice of isotherm is critical in calculating the rate of addition of this volcanism to the oceanic crust. In particular, any feature that has a T_e greater than the maximum depth of the isotherm will be automatically excluded by the algorithm because it cannot be assigned an age at the time of loading. This can be used to remove features such as the Hawaiian-Emperor Seamount Chain that follow a significantly higher isotherm than the rest of the study area and would be assigned anomalous ages if analysed with the same isotherm, but the same effect also excludes up to half the data if the best-fitting isotherm is used, as illustrated in Fig. 6a. To include as many features as possible while minimising errors in the assigned ages, we therefore add one sigma to the best-fitting isotherm, giving 240 °C for SOPITA-influenced lithosphere. This isotherm also helps correct for the bias towards low isotherms that may be caused by repeated episodes of volcanism.

Fig. 6a shows the rate of volcanism in the central Pacific throughout the Jurassic and Cretaceous normalised to correct for the progressive loss of older seafloor through subduction. The rate, which corresponds to the equivalent thickness of volcanism added uniformly over the seafloor in km/Myr, shows two distinct peaks, a well-known one in the Mid Cretaceous, peaking at 110 Ma, (e.g. Larson and Schlanger, 1981), but also a secondary peak of shorter duration near the Jurassic-Cretaceous boundary, peaking at 140 Ma.

To test the results based on the 240 °C isotherm, we use an alternative method that considers only those features with T_e low enough to be formed at or near a spreading ridge. The age of the feature in this case is approximated simply by the age of the underlying seafloor. In previous studies, Cochran (1979) estimated a T_e of 2–13 km at the ridge crest and suggested that the low end of the range was associated with faster spreading rates. Watts et al. (2006)

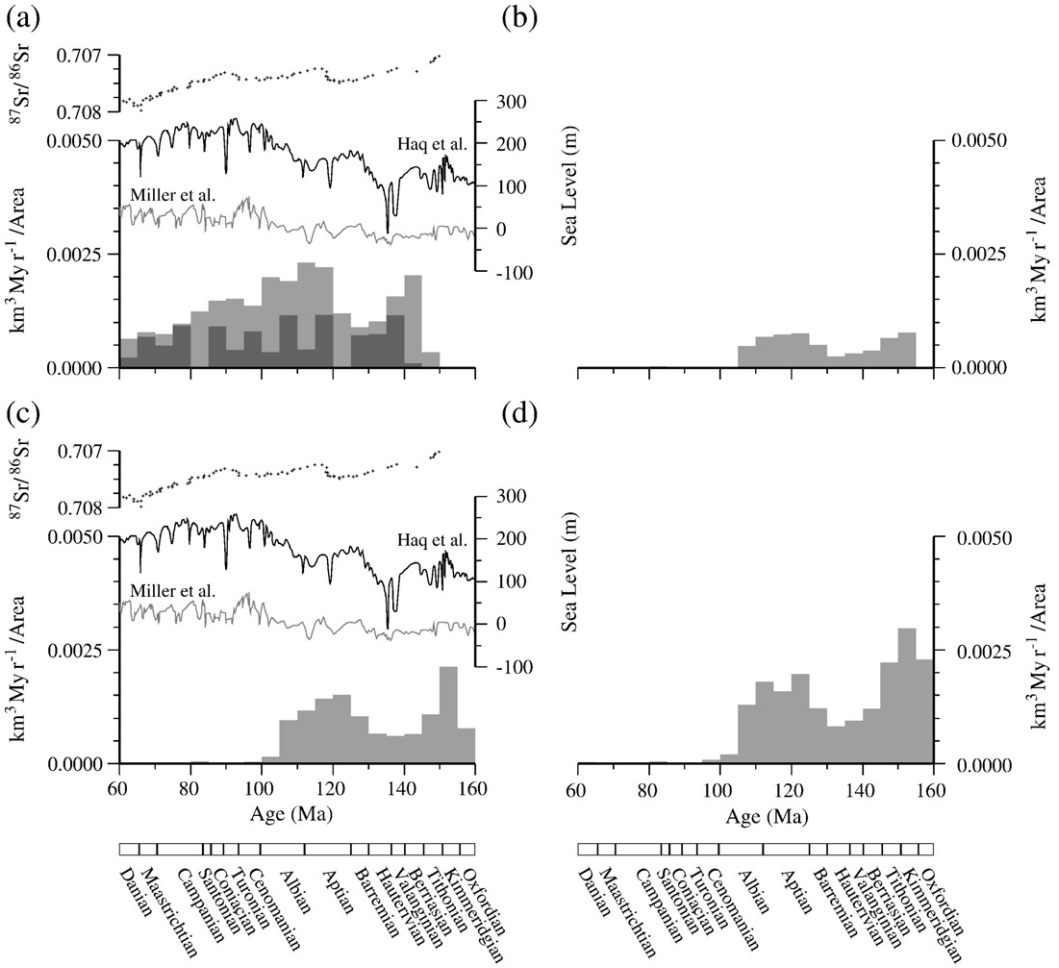

Fig. 6. Area-age corrected rate of volcanism in the Jurassic and Cretaceous based on corrected T_e. The black and grey lines show the sea-level curves of (Haq et al., 1987) and (Miller et al., 2005) respectively, and black crosses indicate the $^{87}Sr/^{86}Sr$ ratio from (Jones and Jenkyns, 2001). (a) Rate using 240 °C controlling isotherm. The results for the 180 °C isotherm are also shown in dark grey to illustrate how the best-fitting isotherm excludes approximately half the data. (b) Rate of on-ridge volcanism assuming $T_e \leq 5$ km at the ridge. (c) Rate of on-ridge volcanism assuming $T_e \leq 7.5$ km. (d) Rate of on-ridge volcanism assuming $T_e \leq 10$ km.

considered features with T_e<12 km to be "on-ridge". We test T_e limits of 5, 7.5, and 10 km to account for the weakening effect of SOPITA and the historically rapid spreading rate in the Pacific. Fig. 6b-d show that all three results include the same two peaks of volcanism seen in the rate calculated using the 240 °C isotherm, although both peaks shift to about 10 Myr earlier, around 120 Ma and 150 Ma respectively.

We caution that our volume and rate estimates are minimum values because seamounts and ocean islands flex the lithosphere, and so there will always be a volume that partially or completely infills the flexure and thus does not appear as positive topographic relief. We use Airy isostasy to estimate that the volume concealed by flexure is two to three times the volume of the topography, assuming a crustal density of 2600-2800 kg/m^3 based on Appendix A.

The addition of submarine volcanism reduces the volume of the ocean basins and displaces water onto the continental margins. We can estimate the magnitude of such a sea-level rise by assuming a global hypsometric curve with a "shelf break" at 500 m, a local isostatic correction for water loading, and densities of 3330 kg/m^3 for mantle and 1030 kg/m^3 for sea water. The Mid Cretaceous volcanism has a total volume of 8×10^6 km^3, which would cause a rise of approximately 20 m. The Late Jurassic peak has a total volume of 4×10^6 km^3, corresponding to a 10 m rise in sea-level. Long-term sea-level will not be affected by the additional volume of volcanic material that is concealed within the flexure because that volume, in effect, displaces mantle rather than sea water.

Fig. 6 shows no obvious correlation between either of the two peaks in volcanism with published sea-level curves derived from the stratigraphic record. Long-term sea-level according to Haq et al. (1987) reaches peaks of approximately 250 m, 160 m, and 140 m above present day 80–100 Ma, 118–128 Ma, and 140–150 Ma respectively. However, the Miller et al. (2005) curve is lower in amplitude and shows no long-lived highstands in the Jurassic or Cretaceous. Given the variability between these two representative curves, we cannot determine whether or not our postulated sea-level rises are reflected in stratigraphic data. One other possible proxy for sea-level change is the $^{87}Sr/^{86}Sr$ ratio, which is believed to be influenced by hydrothermal activity (Jones and Jenkyns, 2001). These data show a peak in the Mid to Late Jurassic and then a slow decrease through the Cretaceous. This is consistent with a high level of volcanism in the Late Jurassic and our suggestion in Fig. 6 that the Late Jurassic may have actually involved a higher rate of volcanic addition than the Early Cretaceous. This apparent correlation between strontium isotopes and volcanic addition rate suggests that on- or near-ridge volcanism at the edges of the accreting Pacific plate may have been accompanied by hydrothermal activity.

Irrespective of these sea-level and isotope proxies, the secondary peak in volcanism is a robust feature of Fig. 6, which tests multiple possible relationships between T_e and age. This peak in submarine volcanism has not been reported before to our knowledge. We attribute this to the limited extent of Jurassic seafloor, much of which is found adjacent to continental margins and thus in regions where the oceanic basement is often obscured by large thicknesses of sediment (e.g. East Coast, USA; West African Margin; Wharton Basin).

We speculate that similar volumes of Late Jurassic volcanism to that found in this paper may have formed on the other limbs of the spreading centres that surrounded the early Pacific plate. These include the Izanagi plate to the northwest, the Farallon plate to the east, and the Phoenix plate to the south. If this is the case, we would expect some modification of the tectonic history of the subduction zones that developed at the margins of the proto-Pacific Ocean. For example, subduction may be impeded by the presence of young, buoyant volcanic features formed at or near a ridge crest. This may be reflected in changes in the polarity of the subduction zone, the degree of coupling between the subducting and overriding plate, or the type and amount of arc volcanism. Indeed, geological field mapping suggests that the margins of the present day Pacific plate experienced a resurgence in tectonic activity during the Late Jurassic to Early Cretaceous (e.g. Nevada orogeny in western North America (Schweickert et al., 1984); widespread volcanism in southern South America (Gust et al., 1985), plutonism in Palmer Land, Antarctica (Leat et al., 1995); back-arc volcanism in Japan (Takashima et al., 2006)), which may reflect the subduction of these postulated Late Jurassic volcanic features.

5. Conclusions

We draw the following conclusions from this study:

1. The moving window admittance technique is a robust way to determine spatial variations in oceanic elastic thickness.
2. Synthetic tests using representative seamounts show that elastic thickness can be recovered to an accuracy of ±5 km for plates up to 30 km thick. For $T_e\leq20$ km, the accuracy increases to ±3 km.
3. The results for the Western Pacific show T_e in the range of 0-50 km with a mean of 9.4 km and a standard deviation of 6.8 km.
4. The T_e structure of the region is dominated by relatively high T_e over the Hawaiian-Emperor Seamount Chain, intermediate values over the Marshall Islands, Gilbert Ridge, and Marcus-Wake Guyots, and low values over the Line Islands, Mid-Pacific Mountains, Caroline Islands, Shatsky Rise, Hess Rise, and Musician Seamounts.
5. Limitations in the spatial resolution of the moving window technique result in a smearing effect, to which we attribute the high values surrounding the Hawaiian-Emperor Seamount Chain and the outer rise seaward of deep-sea trenches.
6. Plots of T_e at sample sites suggest that T_e is to first order controlled by the age of the lithosphere at the time of loading. In areas that backtrack into SOPITA, T_e may be as low as the depth to the 180 ± 120 °C isotherm. In the northern part of the study area including the Hawaiian-Emperor Seamount Chain, T_e correlates with the depth to 310 ± 120 °C.
7. The best-fitting isotherms imply peak rates of volcanism during 100–120 Ma (Early Cretaceous) and 140–150 Ma (Late Jurassic). This corresponds to added volcanic volume of 8×10^6km^3 and 4×10^6 km3 respectively. These added volumes would result in long-term sea-level rises of 20 m and 10 m respectively.
8. The Late Jurassic volcanic event, like the Early Cretaceous event that followed it, appears to have influenced the tectonic evolution of the Pacific plate convergent boundaries, resulting in increased volcanism and orogenesis.

Acknowledgements

Support for LMK was provided by the Clarendon Fund, the Overseas Research Studentship Awards Scheme, and Exeter College, University of Oxford. This manuscript benefited from comments from M. Perez-Gussinye, Alain Bonneville, and an anonymous reviewer.

Appendix A. Recovering the density of the topographic load from admittance

Fitting the observed admittance at wavelengths shorter than the isostatic roll-over, where the topography is largely uncompensated, with an appropriate theoretical admittance (Eq. (5)) recovers an estimated water depth, d, and approximate density contrast across the water-topography interface, $(\rho_l-\rho_w)$. Because ρ_w is known, we thus recover the estimated density of the seafloor topography. Although the recovered depth can be compared with median depths from the input bathymetry grids, no similar data set exists for the density. To analyse the effectiveness of the density estimation, we compute an estimated density for each location using an average of the densities

recovered for each window size weighted by the number of high coherence wavebands from that window, the same weighting factor used in recovering T_e.

Fig. A1 shows the distribution of the recovered densities. In 91% of cases, the fitting method recovers a physically plausible density in the range 1500–3500 kg/m^3. In 80% of cases, the density recovered is between 2000–3000 kg/m^3, with a mode of 2700–2800 kg/m^3 and a median of 2598 kg/m^3. In a small percentage of cases, the fitting method performs poorly, recovering densities outside a reasonable range. Anomalously low densities account for only 0.4% of results, and these densities have a lower bound of ρ_w. In the remainder of cases, the recovered density is anomalously high, occasionally by an order of magnitude or more, and the error in the recovered depth is also large. This occurs when the set of wavebands automatically selected for fitting is inappropriate, generally due to an anomalously high admittance at short wavelength. This restricts the algorithm so that fitting begins at this anomalous wavelength and creates the appearance of rapidly decreasing admittance, which corresponds to deeper water and higher density. With the exception of these anomalous fits, the algorithm shows sufficient accuracy and consistency to recover real regional variations in density.

The wide range of crustal ages in the Western Pacific (110–160 Ma) allows us to examine the relationship between density and crustal age. Fig. A2 shows the age-density frequency distribution of the data binned in intervals of 5 Myr and 100 kg/m^3. The data show a slight increase in density with age, with a best fit of $\rho_l = 2358$ kg/m^3 + 1.4 kg/m^3/Myr for data with a density between 1500–3500 kg/m^3. This result does not depend on the precise choice of limits, although the outlying high density values from algorithm misfits must be removed. We attribute the slight increase in density with age to thermal cooling and compaction as the oceanic crust subsides with age. Carlson and Herrick (1990) obtained an increase of 16 kg/m^3/Myr based on laboratory and in situ drill-hole measurements, which is an order of magnitude higher than our increase. However, their estimates are based on an age range of 0 to 30 Ma. We therefore believe that the rapid increase in density seen in young oceanic crust, attributed by Carlson and Herrick (1990) to hydrothermal alteration, is not seen in Pacific oceanic crust of Mesozoic age.

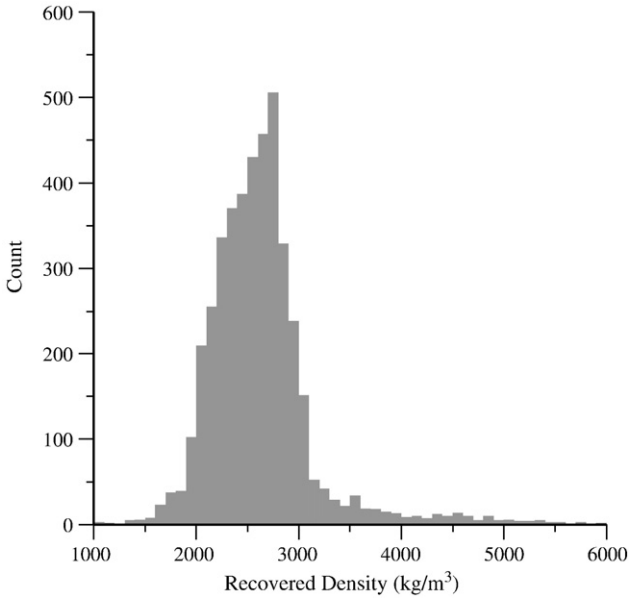

Fig. A1. Histogram of topographic load densities recovered over the western Pacific. The data peak at 2700-2800 kg/m^3 and have a median of 2598 kg/m^3.

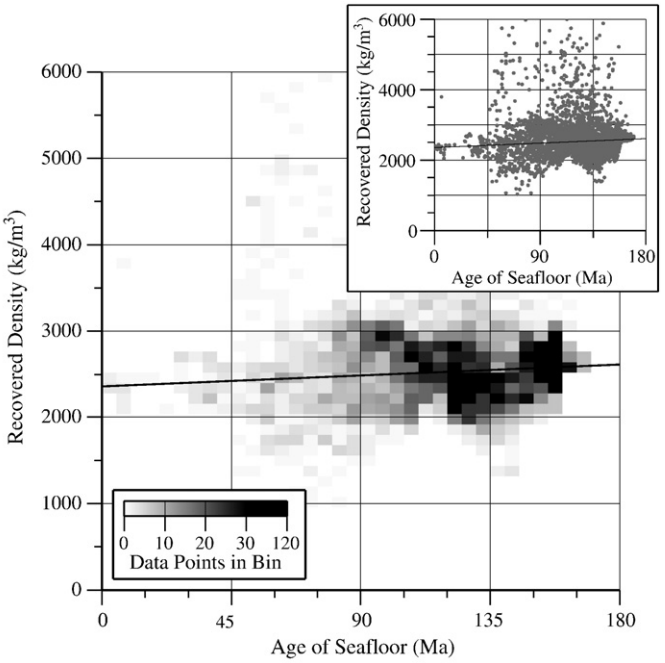

Fig. A2. Frequency distribution of recovered density versus age of underlying lithosphere. The thick black line marks the linear trend of the data, $\rho_l = 2358$ kg/m^3 + 1.4 kg/m^3/Myr, showing a slight increase in density with age. The inset shows the raw, unbinned data with the trend line.

References

Bry, M., White, N., 2007. Reappraising elastic thickness variation at oceanic trenches. J. Geophys. Res.—Solid Earth 112 (B8). doi:10.1029/2005JB004190.

Calmant, S., 1987. The elastic thickness of the lithosphere in the Pacific Ocean. Earth Planet. Sci. Lett. 85 (1–3), 277–288.

Calmant, S., Cazenave, A., 1986. The effective elastic lithosphere under the Cook–Austral and Society Islands. Earth Planet. Sci. Lett. 77 (2), 187–202.

Calmant, S., Cazenave, A., 1987. Anomalous elastic thickness of the ocean lithosphere in the South Central Pacific. Nature 328 (6127), 236–238.

Calmant, S., Francheteau, J., Cazenave, A., 1990. Elastic layer thickening with age of the oceanic lithosphere — a tool for prediction of the age of volcanoes or oceanic crust. Geophys. J. Int. 100 (1), 59–67.

Carlson, R.L., Herrick, C.N., 1990. Densities and porosities in the oceanic-crust and their variations with depth and age. J. Geophys. Res.—Solid Earth Planets 95 (B6), 9153–9170.

Carlson, R.L., Raskin, G.S., 1984. Density of the ocean crust. Nature 311 (5986), 555–558.

Clouard, V., Bonneville, A., 2005. Ages of seamounts, islands, and plateaus on the Pacific plate. In: Foulger, G.R., Natland, J.H., Presnall, D.C., Anderson, D.L. (Eds.), Plates, Plumes, and Paradigms. Special Paper 388. Geological Society of America, pp. 71–90.

Cochran, J.R., 1979. Analysis of isostasy in the world's oceans: 2. Midocean ridge crests. J. Geophys. Res. 84 (B9), 4713–4729.

Davis, A.S., Gray, L.B., Clague, D.A., Hein, J.R., 2002. The Line Islands revisited: New ^{40}Ar/^{39}Ar geochronologic evidence for episodes of volcanism due to lithospheric extension. Geochemistry Geophysics Geosystems 3, 1–28.

Davis, A.S., Pringle, M.S., Pickthorn, L.B.G., Clague, D.A., Schwab, W.C., 1989. Petrology and age of alkalic lava from the Ratak chain of the Marshall Islands. J. Geophys. Res.—Solid Earth Planets 94 (B5), 5757–5774.

Freedman, A.P., Parsons, B., 1986. Seasat-derived gravity over the Musician seamounts. J. Geophys. Res.—Solid Earth Planets 91 (B8), 8325–8340.

Gladczenko, T.P., Coffin, M.F., Eldholm, O., 1997. Crustal structure of the Ontong Java Plateau: modeling of new gravity and existing seismic data. J. Geophys. Res.—Solid Earth 102 (B10), 22711–22729.

Goodwillie, A.M., Watts, A.B., 1993. An altimetric and bathymetric study of elastic thickness in the Central Pacific Ocean. Earth Planet. Sci. Lett. 118 (1–4), 311–326.

Gripp, A.E., Gordon, R.G., 2002. Young tracks of hotspots and current plate velocities. Geophys. J. Int. 150 (2), 321–361.

Gust, D.A., Biddle, K.T., Phelps, D.W., Uliana, M.A., 1985. Associated Middle to Late Jurassic volcanism and extension in southern South America. Tectonophysics 116 (3–4), 223–253.

Haq, B.U., Hardenbol, J., Vail, P.R., 1987. Chronology of fluctuating sea levels since the Triassic. Science 235 (4793), 1156–1167.

Hillier, J.K., Watts, A.B., 2007. Global distribution of seamounts from ship-track bathymetry data. Geophys. Res. Lett. 34 (13). doi:10.1029/2007GL029874.
IOC, IHO, BODC, 2003. Centenary edition of the GEBCO Digital Atlas, published on behalf of the Intergovernmental Oceanographic Commission and the International Hydrographic Organization as part of the General Bathymetric Chart of the Oceans. British Oceanographic Data Centre, Liverpool, U.K.
Jones, C.E., Jenkyns, H.C., 2001. Seawater strontium isotopes, oceanic anoxic events, and seafloor hydrothermal activity in the Jurassic and Cretaceous. Am. J. Sci. 301 (2), 112–149.
Jordahl, K.A., McNutt, M.K., Caress, D.W., 2004. Multiple episodes of volcanism in the southern austral islands: flexural constraints from bathymetry, seismic reflection, and gravity data. J. Geophys. Res.—Solid Earth 109 (B6). doi:10.1029/2003JB002885.
Keating, B.H., Mattey, D.P., Helsley, C.E., Naughton, J.J., Epp, D., Lazarewicz, A., Schwank, D., 1984b. Evidence for a hot spot origin of the Caroline Islands. J. Geophys. Res. 89 (B12), 9937–9948.
Keating, B.H., Mattey, D.P., Naughton, J., Helsley, C.E., 1984a. Age and origin of Truk Atoll, eastern Caroline Islands: geochemical, radiometric age, and paleomagnetic evidence. Geol. Soc. Am. Bull. 95, 350–356.
Koppers, A.A.P., Staudigel, H., 2005. Asynchronous bends in Pacific seamount trails: a case for extensional volcanism? Science 307 (5711), 904–907.
Koppers, A.A.P., Staudigel, H., Wijbrans, J.R., 2000. Dating crystalline groundmass separates of altered Cretaceous seamount basalts by the $^{40}Ar/^{39}Ar$ incremental heating technique. Chem. Geol. 166 (1–2), 139–158.
Lanphere, M.A., Dalrymple, G.B., 1976. K–Ar ages of basalts from DSDP Leg 33; sites 315 (Line Islands) and 317 (Manihiki Plateau. Initial Reports of the Deep Sea Drilling Project, vol. 33. Ocean Drilling Program, pp. 649–652.
Larson, R.L., Schlanger, S.O., 1981. Cretaceous volcanism and Jurassic magnetic-anomalies in the Nauru Basin, Western Pacific Ocean. Geology 9 (10), 480–484.
Leat, P.T., Scarrow, J.H., Millar, I.L., 1995. On the Antarctic Peninsula batholith. Geol. Mag. 132 (4), 399–412.
Lincoln, J.M., Pringle, M.S., Premoli Silva, I., 1993. Early and Late Cretaceous volcanism and reef-building in the Marshall Islands. In: Pringle, M.S., Sager, W.W., Sliter, W.V., Stein, S. (Eds.), The Mesozoic Pacific: Geology, Tectonics, and Volcanism. Geophysical Monograph 77. American Geophysical Union, pp. 279–305.
Lowry, A.R., Smith, R.B., 1994. Flexural rigidity of the Basin and Range—Colorado Plateau–Rocky Mountain transition from coherence analysis of gravity and topography. J. Geophys. Res.—Solid Earth 99 (B10), 20123–20140.
Mahoney, J.J., Duncan, R.A., Tejada, M.L.G., Sager, W.W., Bralower, T.J., 2005. Jurassic–Cretaceous boundary age and mid-ocean-ridge-type mantle source for Shatsky Rise. Geology 33 (3), 185–188.
Maia, M., Arkani-Hamed, J., 2002. The support mechanism of the young Foundation Seamounts inferred from bathymetry and gravity. Geophys. J. Int. 149 (1), 190–210.
McKenzie, D., Bowin, C., 1976. Relationship between bathymetry and gravity in the Atlantic Ocean. J. Geophys. Res. 81 (11), 1903–1915.
McNutt, M., 1979. Compensation of oceanic topography — application of the response function technique to the Surveyor area. J. Geophys. Res. 84 (B13), 7589–7598.
McNutt, M., Fischer, K., 1987. The South Pacific superswell. In: Keating, B., Batiza, R. (Eds.), Seamounts, Islands, and Atolls. In: Geophysical Monograph 43. American Geophysical Union, Washington, DC, pp. 25–34.
McNutt, M., Menard, H.W., 1978. Implications of apparent sea-level history for crustal flexure at Hawaii. Trans.-Am. Geophys. Union 59 (12), 1199-1199.
McNutt, M.K., 1984. Lithosphere flexure and thermal anomalies. J. Geophys. Res. 89 (B13), 1180–1194.
McNutt, M.K., Menard, H.W., 1982. Constraints on yield strength in the oceanic lithosphere derived from observations of flexure. Geophys. J. R. Astron. Soc. 71 (2), 363–394.
Miller, K.G., Kominz, M.A., Browning, J.V., Wright, J.D., Mountain, G.S., Katz, M.E., Sugarman, P.J., Cramer, B.S., Christie-Blick, N., Pekar, S.F., 2005. The phanerozoic record of global sea-level change. Science 310 (5752), 1293–1298.
Müller, R.D., Sdrolias, M., Gaina, C., Roest, W.R., 2008. Age, spreading rates, and spreading asymmetry of the world's ocean crust. Geochemistry Geophysics Geosystems 9.
Natland, J.H., Winterer, E.L., 2005. Fissure control on volcanic action in the Pacific. In: Foulger, G.R., Natland, J.H., Presnall, D., Anderson, D.L. (Eds.), Plates, Plumes and Paradigms. Special Paper 388. Geological Society of America, Boulder, CO, pp. 687–710.
Ozima, M., Honda, M., Saito, K., 1977. $^{40}Ar/^{39}Ar$ ages of guyots in the Western Pacific and discussion of their evolution. Geophys. J. R. Astron. Soc. 51 (2), 475–485.
Ozima, M., Kaneoka, I., Saito, K., Honda, M., Yanagisawa, M., Takigami, Y., 1984. Summary of the geochronological studies of submarine rocks from the Western Pacific Ocean. In: Uyeda, S., Hilde, T.W.C. (Eds.), Geodynamics of the western Pacific–Indonesian region. In: Geophysical Monograph 11. American Geophysical Union, pp. 137–142.
Parmentier, E.M., Haxby, W.F., 1986. Thermal-stresses in the oceanic lithosphere — evidence from geoid anomalies at fracture-zones. J. Geophys. Res.—Solid Earth Planets 91 (B7), 7193–7204.
Parsons, B., Sclater, J.G., 1977. An analysis of the variation of ocean floor bathymetry and heat flow with age. J. Geophys. Res. 82 (5), 803–827.
Pérez-Gussinyé, M., Lowry, A.R., Watts, A.B., Velicogna, I., 2004. On the recovery of effective elastic thickness using spectral methods: examples from synthetic data and from the Fennoscandian Shield. J. Geophys. Res.—Solid Earth 109 (B10). doi:10.1029/2003JB002788.
Pérez-Gussinyé, M., Watts, A.B., 2005. The long-term strength of Europe and its implications for plate-forming processes. Nature 436 (7049), 381–384.
Pringle, M.S., 1993. Age progressive volcanism in the Musician Seamounts. In: Pringle, M.S., Sager, W.W., Sliter, W.V., Stein, S. (Eds.), The Mesozoic Pacific: geology, tectonics, and volcanism. In: Geophysical Monograph 77. American Geophysical Union, pp. 187–215.
Pringle, M.S., Staudigel, H., Duncan, R.A., Christie, D.M., 1993. $^{40}Ar/^{39}Ar$ ages of basement lavas at Resolution, MIT and Wodejebato rocks compared with magneto- and bio-stratigraphic results from ODP Legs 143/144. EOS, Trans. Am. Geophys. Union 73, 353.
Sager, W.W., Pringle, M.S., 1987. Paleomagnetic constraints on the origin and evolution of the Musicians and South Hawaiian Seamounts, Central Pacific Ocean. In: Keating, B., Batiza, R. (Eds.), Seamounts, Islands, and Atolls. In: Geophysical Monograph 43. American Geophysical Union, Washington, DC, pp. 25–34.
Saito, K., Ozima, M., 1976. ^{40}Ar–^{39}Ar ages of submarine rocks from the Line Islands: implications on the origin of the Line Islands. In: Sutton, G.H., Manghnani, M.H., Moberly, R. (Eds.), The Geophysics of the Pacific Ocean Basin and its Margin. In: Geophysical Monograph 19, vol. 19. American Geophysical Union, pp. 369–375.
Saito, K., Ozima, M., 1977. $^{40}Ar/^{39}Ar$ geochronological studies on submarine rocks from western Pacific area. Earth Planet. Sci. Lett. 33 (3), 353–369.
Schlanger, S.O., Garcia, M.O., Keating, B.H., Naughton, J.J., Sager, W.W., Haggerty, J.A., Philpotts, J.A., Duncan, R.A., 1984. Geology and geochronology of the Line Islands. J. Geophys. Res. 89 (B13), 1261–1272.
Schweickert, R.A., Bogen, N.L., Girty, G.H., Hanson, R.E., Merguerian, C., 1984. Timing and structural expression of the Nevadan orogeny, Sierra-Nevada, California. Geol. Soc. Am. Bull. 95 (8), 967–979.
Smith, W.H.F., Sandwell, D.T., 1994. Bathymetric prediction from dense satellite altimetry and sparse shipboard bathymetry. J. Geophys. Res.—Solid Earth 99 (B11), 21803–21824.
Smith, W.H.F., Staudigel, H., Watts, A.B., Pringle, M.S., 1989. The Magellan seamounts — early Cretaceous record of the south Pacific isotopic and thermal anomaly. J. Geophys. Res.—Solid Earth Planets 94 (B8), 10501–10523.
Staudigel, H., Park, K.H., Pringle, M., Rubenstone, J.L., Smith, W.H.F., Zindler, A., 1991. The longevity of the South Pacific isotopic and thermal anomaly. Earth Planet. Sci. Lett. 102 (1), 24–44.
Takashima, R., Nishi, H., Yoshida, T., 2006. Late Jurassic–Early Cretaceous intra-arc sedimentation and volcanism linked to plate motion change in northern Japan. Geol. Mag. 143 (6), 753–770.
Taylor, B., 2006. The single largest oceanic plateau: Ontong Java–Manihiki–Hikurangi. Earth Planet. Sci. Lett. 241 (3–4), 372–380.
Walcott, R.I., 1976. Lithosphere flexure, analysis of gravity anomalies, and the propagation of seamount chains. In: Sutton, G.H., Manghnani, M.H., Moberly, R. (Eds.), The Geophysics of the Pacific Ocean Basin and Its Margin. In: Geophysical Monograph 19. American Geophysical Union, pp. 431–438.
Watts, A.B., 1978. Analysis of isostasy in the world's oceans: 1. Hawaiian–Emperor Seamount Chain. J. Geophys. Res. 83 (B12), 5989–6004.
Watts, A.B., 2001. Isostasy and Flexure of the Lithosphere. Cambridge University Press.
Watts, A.B., Sandwell, D.T., Smith, W.H.F., Wessel, P., 2006. Global gravity, bathymetry, and the distribution of submarine volcanism through space and time. J. Geophys. Res.—Solid Earth 111 (B8). doi:10.1029/2005JB004083.
Watts, A.B., ten Brink, U.S., 1989. Crustal structure, flexure, and subsidence history of the Hawaiian–Islands. J. Geophys. Res.—Solid Earth Planets 94 (B8), 10473–10500.
Watts, A.B., Tenbrink, U.S., Buhl, P., Brocher, T.M., 1985. A multichannel seismic study of lithospheric flexure across the Hawaiian–Emperor Seamount Chain. Nature 315 (6015), 105–111.
Watts, A.B., Zhong, S., 2000. Observations of flexure and the rheology of oceanic lithosphere. Geophys. J. Int. 142 (3), 855–875.
Wessel, P., 1993. A re-examination of the flexural deformation beneath the Hawaiian-Islands. J. Geophys. Res.—Solid Earth 98 (B7), 12177–12190.
Wessel, P., 2001. Global distribution of seamounts inferred from gridded Geosat/ERS-1 altimetry. J. Geophys. Res.—Solid Earth 106 (B9), 19431–19441.
Wessel, P., Haxby, W.F., 1990. Thermal-stresses, differential subsidence, and flexure at oceanic fracture-zones. J. Geophys. Res.—Solid Earth Planets 95 (B1), 375–391.
Winterer, E.L., Natland, J.H., van Waasbergen, R.J., Duncan, R.A., McNutt, M.K., Wolfe, C.J., Silva, I.P., Sager, W.W., Sliter, W.V., 1993. Cretaceous guyots in the northwestern Pacific: an overview of their geology and geophysics. In: Pringle, M.S., Sager, W.W., Sliter, W.V., Stein, S. (Eds.), The Mesozoic Pacific: Geology, Tectonics, and Volcanism. In: Geophysical Monograph 77. American Geophysical Union, pp. 307–334.